Stress Development of a Super-tall Structure During Construction: Field Monitoring and Numerical Analysis

Yong Xia[*]
Assistant Professor,
Department of Civil & Structural Engineering,
The Hong Kong Polytechnic University,
Hung Hom, Kowloon, Hong Kong
Tel: (852) 2766 6066; Fax: (852) 2334 6389
ceyxia@polyu.edu.hk

Yi-qing Ni
Professor,
Department of Civil & Structural Engineering,
The Hong Kong Polytechnic University,
Hung Hom, Kowloon, Hong Kong
Tel: (852) 2766 6004; Fax: (852) 2334 6389
ceyqni@polyu.edu.hk

Peng Zhang
PhD Student,
Department of Civil & Structural Engineering,
The Hong Kong Polytechnic University,
Hung Hom, Kowloon, Hong Kong
Tel: (852) 2766 4019; Fax: (852) 2334 6389
cepzhang@polyu.edu.hk

Wei-yang Liao
PhD Student,
Department of Civil & Structural Engineering,
The Hong Kong Polytechnic University,
Hung Hom, Kowloon, Hong Kong
Tel: (852) 2766 6006; Fax: (852) 2334 6389
weiyang.liao@polyu.edu.hk

Jan-ming Ko
Chair Professor,
Department of Civil & Structural Engineering,
The Hong Kong Polytechnic University,
Hung Hom, Kowloon, Hong Kong
Tel: (852) 2766 5037; Fax: (852) 2356 2682
cejmko@polyu.edu.hk

(*Corresponding author)

ABSTRACT

The safety of the 610 m Guangzhou New Television Tower, due to become China's tallest structure on completion, is an issue that concerns many parties because of the lack of sufficient experience, official design codes, and construction guidelines for such a skyscraper. This paper investigates the strain/stress development of this super-tall structure through the integration of finite element analysis and field monitoring during the construction stage with a particular focus on the following issues: 1) the shrinkage and creep properties of high-strength low-shrinkage concrete; 2) the strain response of the structure to extreme events including typhoons, a major earthquake, and unfavorable construction loads; and 3) the stress evolution of the super-tall structure as construction activity progresses. Field monitoring results demonstrate that the strain responses of the structure to natural hazards are within safe ranges. Finite element model predictions made at different stages of construction are in good agreement with measurement data. The monitoring exercise described in this paper provides the designer, the contractor, and the client with valuable data regarding the safety of the tower. It verifies the effectiveness and importance of monitoring during the construction phase for such a complex super-tall structure.

1 INTRODUCTION

Recent decades have seen the construction of many skyscrapers and the establishment of new building height records from time to time. In mainland China, three skyscrapers of over 600 m in height (including non-structural components) are under construction and a few of over 500 m are being planned. The tallest structure on Earth is currently the Burj Khalifa in Dubai, with a height of 828 m. Although numerical analysis and scaled laboratory experimental techniques have been employed to predict the structural performance of super-tall structures of this type under various loadings, their structural performance under actual construction and service conditions is an issue that has not been investigated in depth to date because of the current shortage of existing, sufficient and mature experience for practical super-tall skyscrapers.

Structural health monitoring (SHM) offers a potential solution as an innovative situ-based laboratory experiment technique that allows for the measurement of a structure's loadings, environmental factors, and responses. The potential benefits of an SHM exercise include (Ko and Ni, 2005; Brownjohn and Pan, 2008): (i) validating the theoretical assumptions made and parameters used in the design, analysis, and laboratory testing phases; (ii) improving the understanding of the structural loading and response mechanisms; (iii) examining the accuracy of the design and design specifications; (iv) enabling inspection of the safety of construction activities and ensuring the structure built satisfies design requirements as closely as possible; and (v) providing real information on the structure following disasters and extreme events to facilitate cost-effective decisions regarding maintenance and management (Adeli and

Jiang, 2006; Jiang and Adeli, 2007; Jiang et al., 2007; Park et al., 2007; Jiang and Adeli, 2008a&b; Moaveni, et al., 2009; Soyoz and Feng, 2009; Umesha et al., 2009; Cruz and Salgado, 2009; Huang, et al., 2009; Adeli and Jiang, 2009; Chen and Liu, 2010; Huang et al., 2010). A well-designed and well-operated SHM system therefore has benefits not only for researchers, but also for the designers, contractors, and clients for a particular structure.

Major applications of SHM have been implemented in the oil industry and in large dams and bridges and have required a great deal of research and practical effort. Residential and commercial structures have received relatively little attention in comparison (Doebling et al., 1996). At present, the majority of monitoring carried out on building structures is aimed at understanding dynamic loadings and responses including those induced by earthquakes and strong winds. For example, three tall buildings in Chicago have been equipped with monitoring systems to compare their wind-induced responses (measured by Global positioning System (GPS) and accelerometers) with predictions made using wind tunnels and finite element (FE) models and discrepancies have been identified (Kijewski-Correa et al., 2006). Brownjohn (2005) compared data from a decade of monitoring of a 280 m office tower in Singapore with design code requirements for both wind and seismic effects, showing that code provisions for both types of loadings are very conservative. Prior studies have reported that more than 150 buildings in California, more than 100 buildings in Japan, and more than 40 buildings in Taiwan have had strong motion monitoring systems for seismic excitation/response measurement and post-earthquake damage assessment installed (Huang and Shakal, 2001; Lin et al., 2003; Huang, 2006). Li et al. (2004) have

taken full-scale measurements on a high-rise building under strong wind conditions and carried out a series of wind-tunnel tests.

For many high-rise structures, the construction stage could be the most critical stage from a safety perspective for two reasons. First, completed structures are normally subject to careful examination through FE analysis and laboratory experiments, whereas structures under construction generally are not. Second, the safety of in-service structures depends to a great extent on conditions during construction. Imperfections of a structure during the construction can lead to permanent additional stresses in the structure in-service that are not taken into account in the design analysis. Although structural safety is usually assured through specification control and safety factors, construction experience and appropriate criteria for super-tall structures are currently lacking. In practice, health monitoring during the construction stage has since become a necessity in bridge engineering (see, for example, Shahawy and Arockiasamy, 1996; Lin et al., 2005). Although numerical methods have been developed to predict the load distribution of building structures during construction (Stivaros and Halvorsen, 1990; Fang et al., 2001; Nunez and Boroschek, 2010), systematic monitoring during the construction of residential and commercial buildings is still rare. One possible reason for this is that bridges are generally owned by public authorities, while most buildings belong to private companies or individuals.

An additional benefit of construction monitoring is that it can provide valuable data of the structure as-built and can be integrated with long-term in-service monitoring. As a result, real strain data can be obtained and evaluated rather than only relative strain data if SHM equipment is installed after the construction phase has been completed. This

5

aspect has been neglected in previous SHM exercises, possibly because construction monitoring is usually conducted by contractors, while long-term in-service monitoring is carried out by the structural management sector. Different concerns and interests of these two groups usually lead to their respective monitoring exercises are performed separately. Nevertheless, the Guangzhou New Television Tower (the "Guangzhou New TV Tower") provides a unique opportunity integrate in-construction monitoring with in-service monitoring (Ni et al., 2009).

This paper focuses mainly on the monitoring and analysis of strain and stress in the Guangzhou New TV Tower during the construction stage. The paper addresses the following issues: 1) the establishment of shrinkage and creep models for concrete based on field experiments and their comparison with ACI formulae; 2) the calculation of principal stresses in critical components based on strains measured during extreme loading cases including a long-distance earthquake, typhoons, and construction activities; and 3) tracking of the stress development of the tower throughout the entire 2-year construction stage through finite element (FE) numerical analysis and field monitoring verification. The practical monitoring exercise described in this paper demonstrates how an SHM system can benefit interested parties including the designer, the contractor, the client, and the public.

2   THE GUANGZHOU NEW TV TOWER AND THE STRAIN MONITORING SYSTEM

2.1   *Guangzhou New Television Tower*

The Guangzhou New TV Tower currently nearing completion is a super-tall structure with a height of 610 m and is the tallest building of its type in the world. It is being built to broadcast the 16th Asian Games due to be held in Guangzhou from November 12 to 27, 2010. It will subsequently be used as office space and for entertainment, dining, tourism, and the transmission of television and radio programs. The structure consists of a main tower (454 m) and an antenna mast (156 m). Fig. 1 illustrates the perspective view of the tower in July 2009 when the entire structure was topped out and non-structural construction activities (such as the erection of a curtain wall and interior decoration) were still ongoing.

This tube-in-tube structure comprises a reinforced concrete inner tube (core) and a steel outer frame tube. Fig. 2 shows the inner tube and outer tube separately for clarity. There are 36 floors and four levels of connection girders linking the inner tube with the outer tube. The basement has two floors with a total height of 10 m and an expanded floor area of about 167 m × 176 m. Pile foundations are being employed for the structure and Chinese design codes are being implemented.

The outer tube consists of 24 concrete-filled tube (CFT) columns uniformly spaced in an oval configuration and inclined in the vertical direction that are connected by hollow steel rings and braces. The dimensions of the oval decrease from 60 m × 80 m at the underground level (at a height of -10 m) to the minimum of 20.65 m × 27.5 m at the height of 280 m before increasing to 40.5 m × 54 m at the top of the tube (454 m). The top oval is rotated clockwise by 45 degrees with respect to the bottom oval in the

horizontal plane. There are 46 steel 'ring' beams linking the CFT columns with an inclination angle of 15.5 degrees to the horizontal plane and non-uniform intervals in the vertical direction. The hollow steel braces connect the beam-column joints.

The inner RC tube is also an oval with constant dimensions of 14 m × 17 m, while its centroid differs from that of the outer oval. The thickness of the tube varies from 1.0 m at the bottom to 0.4 m at the top. C80 grade high-strength low-shrinkage concrete that meets the Chinese code GB 50010 2002 and has characteristic cube strength of 50.2 MPa is poured below the height of 36 m and the concrete grade gradually decreases to C45 (characteristic cube strength = 29.6 MPa) at the top of the tower. The inner tube is mainly used for vertical transportation and holds six lifts, stairs, and a few facility rooms where pipes and cables are installed. An antenna mast stands on top of the inner tube and is made of steel lattice.

Fig. 2 also shows the plan of a typical floor that is made of a composite decking with profiled steel sheet as the permanent bottom formwork for a 150 mm reinforced concrete slab. It can be seen that the floor is not directly attached to the outer tube. Radiating steel girders in the floor, not shown in the figure, stretch out from the bottom of the floor and are connected by a pin to the corresponding CFTs in the outer tube through a bolt in each CFT. The other end of each girder is welded to the inner tube through an embedded steel corbel with a connection that provides moment resistance. The floor perimeter is enclosed by a curtain wall system (inside the outer tube) attached to the slab. Most of the inner tube is exposed to the atmosphere, the only exception being the floors enclosed by the curtain wall. There are four levels of connection girders

without a floor at heights of about 204 m, 230 m, 272 m, and 303 m that join the inner tube to the outer tube.

Although the non-symmetric, non-uniform, and twisted geometry configuration makes the structure interesting and attractive from an aesthetic perspective, it also makes it mechanically complex. In particular, it lacked adequate connections between the inner tube and the outer tube during the construction stage. Given that full-scale testing was not feasible, the structural performance of the tower and the strains and stresses on some critical components under extreme loadings during the construction stage in particular is a matter of concern to the contractor, the designer, and the client.

2.2   The SHM system

To ensure the safety of the structure both during construction and over the long term once the building goes into service, a consortium made up of researchers from the Hong Kong Polytechnic University (located in Hong Kong) and Sun Yat-Sen University (located in Guangzhou) installed a sophisticated SHM system consisting of more than 700 sensors of 16 different types in the tower. Ni et al. (2009) have described this system in detail. Noteworthy features of this system include the strain and temperature monitoring sub-system employed during the construction stage comprising substations, vibrating wire strain gauges, and thermal sensors distributed along 12 sections at different heights. Based on a modular design concept (Ko and Ni, 2005), each substation collects signals from the surrounding sensors, digitizes the analog signals, and transmits the data to a control room. Critical sections with a large axial compression ratio are selected via a preliminary FE analysis. Fig. 3 shows 12 sections at the heights

9

of 32.8 m, 100.4 m, 121.2 m, 173.2 m, 204.4 m, 230.4 m, 272.0 m, 303.2 m, 334.4 m, 355.2 m, 376.0 m, and 433.2 m on the inner concrete tube. It is noted that sections five through eight correspond to the four levels at which connection girders are placed.

In the inner tube, a 45-degree strain rosette was installed at four points (denoted as points 1 ~ 4 in Fig. 4) in each critical section with each rosette consisting of three Geokon vibrating wire strain gauges (Geokon 4200) to measure the strain and temperature of the concrete wall. Fig. 4 shows the positions of the strain gauges in the plan and Fig. 5 shows the installation of a typical strain rosette in the RC wall of the inner tube with firm protection. Fig. 5(a) is a photograph of an original Geokon 4200 gauge. To measure the strain of the concrete rather than that of the rebar, the vibrating wire strain gauges were coated using two semi-cylinders with a diameter of 40 mm with concrete being poured into the day before the concrete was poured. To minimize the shrinkage effect, the concrete used for coating is the same as that used in the structure. About seven to eight hours later, the semi-cylinders were removed and the coated gauges were ready for installation as shown in Fig. 5(b). All the gauges were inspected and tested using a portable readout box. A strain rosette was then attached to the rebars (Fig. 5(c)) to avoid movement while concrete was poured and to measure the strain in three directions at each point. The cables were then protected by stainless galvanized steel pipes embedded in the concrete floor (Fig. 5(d)). This protects the cables from causal damage. The strain and temperature at each of the points were taken in the days immediately after the concrete was poured. During the first few days, the temperature varied significantly due to hydration. Strain also developed due to initial shrinkage and stress redistribution, phenomena which are hard to predict. The strain reading taken

after 5-7 days when the temperature and strain readings became stable can be regarded as the initial strain of the concrete without external load.

The SHM project commenced in June 2007 once the inner tube had been constructed to a height of about 120 m. The 121.2 m section was first equipped with gauges embedded inside the inner core wall. Embedded gauges were then installed in the upper sections as construction activity progressed, while sensors (Geokon 4000) were installed on the exterior surface of the core wall in the 32.8 m and 100.4 m sections as concrete construction had been completed by that time. The surface gauges were attached to two grouted concrete mounting blocks on the wall as suggested in the installation guidelines (Geokon 4000). However, as discussed later, monitoring results show that data recorded in the two lower sections are much noisier than those taken from the other gauges embedded inside the core wall.

As the vibrating wire strain gauge cannot measure the dynamic strain, the present system measures the strain once per minute (at a sampling frequency of 1/60 Hz). During construction, the strain and temperature data were collected and temporarily stored in each substation and were wirelessly transmitted to the control room in real time. The wireless data transmission system consists of three parts: a WiFi router, a wireless bridge, and an antenna. The system can transmit data at rates of up to 100 Mps and has a maximum transmission distance of 2 km. Network Time Protocol is used to synchronize the substations.

Although the strain gauges and cables have been carefully handled and protected, tests show that seven of the 144 sensors (5%) did not function once construction of the

structure had been completed. As the sensors and cables are embedded in concrete, the reason for this damage is unknown.

3   SHRINKAGE AND CREEP OF CONCRETE

The raw data obtained from a vibrating wire strain gauge is the frequency of the vibrating wire embedded in the gauge. This frequency is converted into strain across the gauge by compensating for the temperature measured by an embedded thermocouple. It is noted that the strain of the wire can be regarded as the strain of the structure at the sensor point and includes both strain due to external forces and strain induced by the shrinkage and creeping of concrete. These shrinkage and creep effects must therefore be removed and the remaining strain can be regarded as the net strain due to external loads only. The net strain is used to calculate the real stresses at a particular point.

As noted earlier, the structure is made of high-strength low-shrinkage concrete. Consequently, its shrinkage and creep may differ from predictions made using empirical formulae that are based on normal concrete under standard conditions specified in ACI 209 R-92 (1992). A series of experiments were conducted to obtain more accurate estimates of the time-dependent shrinkage and creeping properties of the tower. According to the Chinese code on shrinkage experiments (BGJ 82, 1985), two rectangular parallelepiped specimens with dimensions of 100 mm × 100 mm × 515 mm were made on site. A vibrating wire gauge was embedded inside each specimen to measure the strain time history under outdoor conditions. The specimens were then placed on the floors beside the shear wall so they were under the same conditions as

those affecting the structure. Fig. 6 shows the shrinkage strain measured at the two grade C60 specimens together with the predictions suggested by the ACI code (ACI 209 R-92, 1992). The figure clearly shows that the ACI code overestimates the shrinkage strain of the concrete used in the tower. The measurement data are fitted with the ACI formulae as

$$(\varepsilon_{sh})_t = \frac{t}{\alpha + t}(\varepsilon_{sh})_u \tag{1}$$

$$(\varepsilon_{sh})_u = \beta k_1 k_2 k_3 k_4 k_5 k_6 k_7 \tag{2}$$

where $(\varepsilon_{sh})_t$ is the shrinkage strain at time t, $(\varepsilon_{sh})_u$ is the final shrinkage strain, α and β are two parameters to fit, and $k_1 \sim k_7$ are the coefficients representing various conditions including curing, ambient humidity, size, fine aggregate percentage, cement content, and air content. The seven coefficients ($k_1 \sim k_7$) have the same form as those of the ACI formulae (ACI 209 R-92, 1992) and only α and β are fitted. The fitted values of α for the two specimens are 15.5 and 13.3 and those for β are 433 με and 389 με, giving average values of 14.4 and 411 με, respectively, much smaller than the ACI code values of 35 and 780 με.

In a similar manner, creep tests were conducted on a creep machine in a laboratory. These tests started from a concrete age of 28 days as suggested in BGJ 82 (1985). The specimens were loaded at the stress of 27% of the characteristic cube strength (equivalent to 40% of the design compressive strength according to the Chinese code GB 50010, 2002). Fig. 7 shows the creep coefficient measured at the two specimens and the ACI code predictions. The results clearly show that the ACI code also overestimates the creep strain of the concrete used in the tower. The measurement data are fitted with the ACI creep formulae (ACI 209 R-92, 1992) as

$$v_t = \frac{t^{0.6}}{\delta + t^{0.6}} v_u \qquad (3)$$

$$v_u = \gamma f_1 f_2 f_3 f_4 f_5 f_6 f_7 \qquad (4)$$

where v_t is the creep coefficient at the loading age of t, v_u is the final creep coefficient, δ and γ are two parameters to fit, and $f_1 \sim f_7$ are the coefficients representing various conditions including curing, size, cement percentage, and air. The seven coefficients ($f_1 \sim f_7$) have the same form as those of the ACI formulae and only δ and γ are fitted. The fitted values of δ for the two specimens are 1.952 and 1.537 and the fitted values for γ are 0.558 and 0.542, giving average values of 1.75 and 0.55, respectively, much smaller than the ACI code values of 10 and 2.35.

The fitted shrinkage model and the creep model were then used to calculate the shrinkage and creep strain of the concrete components of the tower according to concrete grade, age, and loading level. The net strain was then calculated by deducting the shrinkage and creep from the total strain measured. In the rest of the paper, stress is calculated from the net elastic strain without further clarification.

4   STRAIN AND STRESS RESPONSES DUE TO EXTREME LOADINGS

To evaluate the safety of the tower structure during construction, strain data measured under extreme cases were analyzed and employed to calculate the principal stress at each point. During the calculation of the principal stress, the modulus of concrete was adjusted to the age and grade of concrete according to ACI 209 R-92 (1992):

$E_{ct} = 0.043\left[w^3\left(f_c^{'}\right)_t\right]^{1/2}$, where w is the unit weight of concrete in kg/m^3 and $\left(f_c^{'}\right)_t$ the compressive strength of concrete in MPa. The extreme cases including construction activity, typhoon events, and an earthquake are respectively examined and described in the following sections.

4.1 Construction activity

The inner tube of the tower was constructed earlier than the outer tube of the tower according to progress in construction. The completed inner tube is higher than the outer tube to allow cranes attached to the inner wall to lift CFTs and other components into place. As a result, the top section of the inner tube can be treated as a cantilever part and its bottom is supported by the floors (or connection girders) connected to the outer tube. Fig. 8a illustrates an extreme situation when the inner tube is about 60 m higher than the outer tube and the two tubes are linked by the connection girders at a height of 204 m (which is denoted as the first connection level). There are four connection levels in total as illustrated in Fig. 2. In this situation, the stresses at the first connection level (the bottom of the cantilever part) were of concern to the designer and the contractor and needed to be examined carefully.

Fig. 8b plots the variations in the principal stresses at the first connection level in a single day at this critical stage. As there was no other special loading acting on the structure, the variations in the stresses were attributed to normal construction events and most likely reflect crane activity. It was observed that from 14:00 to 15:00, the compressive stress at point 4 increased while that at point 2 decreased, which might indicate that one crane was erecting a heavy component in this plane and caused both

15

compression at point 4 and tension at point 2. Subsequently, the compressive stress at point 2 rose while that at point 4 dropped, observations that might be due to the crane moving to the other point. A few similar cycles can be observed in the figure. This variation is the most significant among those observed during the normal construction stage. As the variation in stress was less than 0.3 MPa, the construction activity undertaken can be regarded as safe. In addition, this type of monitoring data can potentially be applied to the automatic identification of key construction activities, a topic that has been widely discussed in the construction community (Chi et al., 2009).

4.2   *Typhoon event*

The tower is located in a typhoon-prone area in which four typhoons struck in 2008. The real-time monitoring system installed in the tower recorded structural responses to all of these typhoon events. For example, Typhoon Neoguri hit the Guangzhou area on April 19, 2008. The anemometer installed at the top of the tower (at a height of 375 m) measured the 2-minute mean wind speed as 23.3 m/s and the 3-second maximum wind speed as 28.1 m/s. Fig. 9 plots the 2-minute mean wind speed and shows the corresponding wind rose diagram. It can be seen that the maximum wind speed occurred between 18:00 and 19:00.

Fig. 10 shows the vertical strains measured at point 2 and point 4 on the 121.2 m cross-section during the same typhoon. It can be observed that large strain variations occurred between 18:00 and 19:00 when the wind speed reached its maximum. To illustrate the typhoon responses at various heights on the tower, changes in the principal stresses recorded at four monitoring points on different sections of the tower are compared in

Fig. 11. It is noted that almost all the maximum variations in the stresses occurred between 18:00 and 20:00. All of the principal stresses at point 1 and point 4 decreased (compression went up) as a result of the typhoon, while those at point 2 and point 3 increased (compression dropped). This is because the typhoon was blowing from the southeast to the northwest as indicated by the wind rose diagram in Fig. 9. Fig. 11 also shows that the 303.2 m section (corresponding to the fourth connection level) experienced the largest variation in stress on the day the typhoon struck. At that time, the inner tube had been constructed to a height of 370 m and the outer tube had risen to a height of about 310 m. The fourth connection level therefore acted as the bottom of the cantilever and the principal stresses at the four monitored points varied by about 0.48 MPa, 0.32 MPa, 0.28 MPa, and 0.38 MPa, respectively. The variation in stress as a percentage of total stress at each of the four points was about 16%, 14%, 14%, and 16%, respectively. The stresses measured at all these points were within linear range, indicating no damage has been occurred during this strong wind.

4.3   Earthquake event

The devastating Wenchuan Earthquake that hit southwestern China has again highlighted the need for real-time monitoring of important and critical civil structures during major hazardous events. Despite extensive research conducted in the field of earthquake engineering, the real-time performance of super-tall building structures under strong earthquake loading is monitored only to a limited extent.

The Wenchuan Earthquake occurred at 14:28 on 12 May 2008. The monitoring system of the Guangzhou New TV Tower observed significant strain variation at about 14:35, 7

minutes after the earthquake struck. The distance between Wenchuan and Guangzhou is about 1,325 km and the wave propagation was calculated at around 3,150 m/s. Fig. 12 shows the vertical strains measured at the 121.2 m cross-section during the earthquake. It can be observed that the peak-peak variation in strain was less than 5 μɛ. A comparison of difference levels shows that the maximum variation in the principal stresses at the middle section (173.2 m) was larger than those at the bottom and at the top of the tower as shown in Fig. 13. This indicates that the earthquake loading had a more significant effect on the middle than it did on the bottom and the top of the structure, which is different from the response pattern observed under the wind loading discussed in the last section. This may be due to different modes being excited under the two different types of loading.

It is noted that the recorded strains may be smaller than the actual maximum values due to the low sampling frequency. As the seismic sensors, accelerometers, and dynamic strain gauges hadn't been installed at the construction monitoring stage, detailed information of the earthquake and dynamic responses of the structure are not available. Detailed earthquake analysis is required during the long-term monitoring.

5   EVOLUTION OF STRESSES DURING CONSTRUCTION

Construction activity for the entire tower will have lasted for two and a half years by the time the tower is completed. Tracking changes in and the evolution of strains and stresses has several benefits: 1) it allows the contractor and the designer to be aware of stress levels in different components of the structure at different stages of construction; 2) it allows for the absolute strains and stresses in structural components to be obtained

after the structure has been completed rather than merely giving the relative strains and stresses as in the usual long-term monitoring systems; 3) measurement data and FE predictions can be compared to verify the design model and design assumptions.

As the monitoring system described in this paper can continuously capture the strain responses of the tower at different stages, the strains and the stresses can be compared with the corresponding FE model predictions. Ten construction stages were analyzed starting from July 2007 when the first set of data was measured by the SHM system to July 2009 when the main structural components were completed. Fig. 14 shows photographs of the tower at different stages of construction. The measured strain data were processed by removing the effects of shrinkage and creep as previously described. To minimize the uncertainty arising from the measurement and variation in construction activity, the strains measured in one week were averaged to produce the measurement data and these data were used to calculate the principal stresses during the study period.

FE models were constructed using SAP2000 Version 11.0 (SAP2000, 2006) according to the structural components under construction at the time (see Fig. 14). In these models, two-node three-dimensional Euler beam elements with six degrees of freedom (DOFs) at each node were employed to model the outer structure, the antenna mast, and the connection girders between the inner and outer structures. Four-node and three-node shell elements with six DOFs at each node were used to model the shear walls of the inner structure and the floor decks. All of the nodes in the basement were fixed in six directions. The full model at the final stage contains 122,476 elements, 84,370 nodes, and 505,164 DOFs in total. Only the dead load of the completed components and the mass of major construction facilities including cranes and the construction platform

were included in the models. The modulus of concrete was adjusted to the age of the concrete and to each grade of concrete according to ACI 209 R-92 (1992).

At different stages, the stresses of the structure are obtained via linear analysis and compared with the measurements. Fig. 15 compares the calculated stresses of point 2 at different heights in July 2009 with the measured counterparts. It can be seen that the model predictions and the field measurements are generally in good agreement although and the average discrepancy is about 10%. The discrepancy may be due to the uncertainty of the measurement and the difference between the FE model and the actual structure constructed. For example, the construction error of the large-scale structure results in additional stresses that are difficult to model in the numerical analysis. Non-uniform temperature distribution throughout the structure also causes thermal stresses at components, which is not considered at the moment. In addition, inaccuracy in the material properties contributes to discrepancy of results. Considering these factors, the discrepancy is acceptable. It is also observed that the stress differences in the sections close to the connection girders were relatively large due to the concentration of stress in regions where the inner tube and the outer tube interact. This suggests that more sensors should have been installed in the regions. The stresses in the lower sections were generally larger than those in the upper sections, with the exception of those at 355.2 m. It is observed the thickness of the wall above 339.6 m decreased from 500 mm to 400 mm (a 20% reduction), whereas the dead load at 355.2 m decreased by less than 20% in comparison with that observed at 334.4 m. Consequently, the stress increased a little at 355.2 m.

Fig. 16 illustrates the evolution of principal stress at point 2 at the 121.2 m level as construction activity progressed. Again, the model predictions match the measurement data well. It is observed that the principal stress increased monotonically as construction work proceeded.

Fig. 17 illustrates the vertical strains measured by the gauge at point 2 at the 32.8 m and 121.2 m levels. As noted previously, the strain gauges at the 32.8 m and 100.4 m sections were attached to the grouted mounting blocks on the exterior surface of the wall, while all the other strain gauges (above 121.2 m) were embedded inside the wall. The compressive strain data measured by the embedded sensor gradually rose from -110 $\mu\varepsilon$ to -170 $\mu\varepsilon$ over six months, thereby verifying the progress made in construction. However, the data measured by the surface sensor vary significantly and do not show a clear increasing trend during the study period. One reason for this is that the raw strain measured by the vibrating wire includes the strain due to temperature change measured by the thermocouple embedded in the vibrating wire. This thermocouple measured the ambient air temperature rather than the temperature of the concrete wall. This resulted in incorrect strain data when an incorrect temperature was employed to remove the temperature effect from the raw strain. Due to this reason, the strain data measured by the sensors at the two lowest levels are not reported in this paper.

6 CONCLUSIONS

This paper discusses a sophisticated structural health monitoring system established in the Guangzhou New Television Tower, a new super-tall structure that is nearing

completion. The strain and temperature monitoring sub-system installed as the tower was being constructed comprises 12 substations placed in different sections of the structure, each of which contains 12 vibrating wire strain gauges and four thermal sensors. The two-year strain and stress monitoring exercise undertaken during the construction stage shows that the performance of the sensors and the data acquisition system are satisfactory. In particular, the following conclusions can be drawn.

1) The shrinkage and creep models fitted using data from the field experiments have similar forms to the traditional models adopted by ACI, whereas the rates of shrinkage and creep in the high-strength low-shrinkage concrete used in the structure are much lower than those seen in ordinary concrete.

2) After removing the effects of shrinkage, creep and temperature-induced strain, the structural stresses measured under various types of extreme loads (including typhoons and a major earthquake) were within the value ranges specified in the design, thereby confirming the safety of the tower during the construction period.

3) The structural strain responses due to Typhoon Neoguri were generally larger than those caused by a far-distance earthquake and daily construction activities. The maximum response to the typhoon occurred at the upper section while that to the earthquake occurred at the middle section.

4) The strains and stresses measured at different points and during ten stages of construction were calculated using fine FE models. The results show a good level of agreement with the field data and thus verify the accuracy of the design model;

5)   The vibrating wire strain gauges embedded inside the concrete wall provide more reliable and stable data than those installed on the surface of the concrete wall.

The monitoring exercise discussed in this paper not only provides valuable information on the stress and strains of the structure during construction, but also represents a baseline for long-term monitoring in the near future because real strain data are available. This is an improvement on normal circumstances in which only relative strain data are available due to the SHM being installed after the construction phase is finished.

ACKNOWLEDGMENTS

REFERENCES

ACI 209 R-92, (1992), *Prediction of Creep, Shrinkage, and Temperature Effects in Concrete Structures*, America Concrete Institute, MI, USA

Adeli, H. and Jiang, X. (2006), Dynamic Fuzzy Wavelet Neural Network Model for Structural System Identification, *Journal of Structural Engineering*, ASCE, Vol. 132, Vol. 1, pp. 102-111.

Adeli, H. and Jiang, X. (2009), *Intelligent Infrastructure – Neural Networks, Wavelets, and Chaos Theory for Intelligent Transportation Systems and Smart Structures*, CRC Press, Taylor & Francis, Boca Raton, Florida.

Brownjohn, J. M. W. (2005), Lateral Loading and Response for a Tall Building in the Non-Seismic Doldrums, *Engineering Structures*, 27 (12), 1801-1812.

Brownjohn, J. M. W. and Pan, T. C. (2008), Identifying loading and response mechanisms from ten years of performance monitoring of a tall building, *Journal of Performance of Constructed Facilities, ASCE*, 22 (1), 24-34.

Chen, B. and Liu, W. (2010), Mobile Agent Computing Paradigm for Building a Flexible Structural Health Monitoring Sensor Network, *Computer-Aided Civil and Infrastructure Engineering*, 25:7, 504-516.

Chi, S., Caldas, C. H., and Kim, D. Y. (2009), A Methodology for Object Identification and Tracking in Construction based on Spatial Modeling and Image Matching Techniques, *Computer-Aided Civil and Infrastructure Engineering*, 24 (3), 199-211.

Cruz, P.J.S. & Salgado, R. (2009), Performance of vibration-based Damage Detection Methods in Bridges, *Computer-Aided Civil and Infrastructure Engineering*, 24(1), 62-79.

Doebling, S. W., Farrar, C. R., Prime, M. B. and Shevitz, D. W. (1996), Damage Identification and Health Monitoring of Structural and Mechanical Systems From Changes in Their Vibration Characteristics: A Literature Review, *Los Alamos National Laboratory Report* LA-13070-MS.

Fang, D. P., Zhu, H. Y., Geng, C. D. and Liu, X. L. (2001), On-site measurements of structural characteristics of reinforced concrete buildings during construction, *ACI Structural Journal,* 98 (2), 157–163.

GB 50010, (2002), *Code for Design of Concrete Structures*, National Standard of PRC (in Chinese), Beijing, China.

GBJ 82, (1985), *Experimental methods of long-term performance and durability of common concrete*, National Standard of PRC (in Chinese), Beijing, China.

Geokon 4200, http://www.geokon.com/products/datasheets/4200.pdf

Geokon 4000, http://www.geokon.com/products/datasheets/4000.pdf

Huang, C.S., Huang, S.L., Su, W.C., and Wu, C.L. (2009), Identification of time-variant modal parameters using TVARX and low-order polynomial function, *Computer-Aided Civil and Infrastructure Engineering,*" 24:7, pp. 470-491.

Huang, M. J., Shakal, A. F. (2001), Structure Instrumentation in the California Strong Motion Instrumentation Program, *Strong Motion Instrumentation for Civil Engineering Structures*, 373, 17-31.

Huang, R.Y., Mao, I.S., and Lee, H.K. (2010), Exploring the Deterioration Factors of Bridges: A Rough Set Theory Approach, *Computer-Aided Civil and Infrastructure Engineering*, 25:7.

Huang, M. J. (2006), Utilization of strong-motion records for post-earthquake damage assessment of buildings, *Proceedings of the International Workshop on Structural*

Health Monitoring and Damage Assessment, Taichung, Taiwan, December 14-15, 2006, IV1-IV29.

Jiang, X. and Adeli, H. (2005), Dynamic Wavelet Neural Network for Nonlinear Identification of Highrise Buildings, *Computer-Aided Civil and Infrastructure Engineering*, 20 (5), 316-330.

Jiang, X. and Adeli, H. (2007), Pseudospectra, MUSIC, and Dynamic Wavelet Neural Network for Damage Detection of Highrise Buildings, *International Journal for Numerical Methods in Engineering*, Vol. 71, No. 5, 606-629.

Jiang, X. and Adeli, H. (2008a), Dynamic Fuzzy Wavelet Neuroemulator for Nonlinear Control of Irregular Highrise Building Structures, *International Journal for Numerical Methods in Engineering*, Vol. 74, No. 7, pp. 1045-1066.

Jiang, X. and Adeli, H. (2008b), Neuro-Genetic Algorithm for Nonlinear Active Control of Highrise Buildings, *International Journal for Numerical Methods in Engineering*, Vol. 75, No. 7, pp. 770-786.

Jiang, X., Mahadevan, S., and Adeli, H. (2007), Bayesian Wavelet Packet Denoising for Structural System Identification, *Structural Control and Health Monitoring*, 14 (2), 333-356.

Kijewski-Correa, T., Kilpatrick, J., Kareem, A., Kwon, D. K., Bashor, R., Kochly, M., Young, B.S., Abdelrazaq, A., Galsworthy, J., Isyumov, N., Morrish, D., Sinn, R. C., and Baker, M. F. (2006), Validating Wind-Induced Response of Tall Buildings: Synopsis of the Chicago Full-Scale Monitoring Program, *Journal of Structural Engineering, ASCE*, 132 (10), 1509-1523.

Ko, J. M. and Ni, Y. Q. (2005), Technology developments in structural health monitoring of large-scale bridges, *Engineering Structures*, 27 (12), 1715-1725.

Li, Q. S., Wu, J. R., Liang, S. G., Xiao, Y. Q., and Wong, C. K. (2004), Full-scale measurements and numerical evaluation of wind-induced vibration of a 63-story reinforced concrete tall building, *Engineering Structures,* 26 (12), 1779-1794.

Lin, C. C., Wang, C. E., Wang, J.F. (2003), On-line building damage assessment based on earthquake records, *The First International Conference on Structural Health Monitoring and Intelligent Infrastructure*, Tokyo, Japan, November 13-15, 2003, 551-559.

Moaveni, B., Conte, J.P., and Hemez, F.M. (2009), Uncertainty and Sensitivity Analysis of Damage Identification Results Obtained Using Finite Element Model Updating, *Computer-Aided Civil and Infrastructure Engineering*, 24:5, pp. 320-334.

Lin, Y. B., Pan, C. L., Kuo, Y. H., Chang, K. C. and Chern, J. C. (2005), Online onitoring of highway bridge construction using fiber Bragg grating sensors, *Smart Materials and Structures*, 14 (5), 1075-1082.

Ni, Y. Q., Xia, Y., Liao, W. Y., and Ko, J.M. (2009), Technology Innovation in Developing the Structural Health Monitoring System for Guangzhou New TV Tower, *Structural Control and Health Monitoring*, 16 (1), 73-98.

Nunez, T. R., and Boroschek, R. L., (2010), Modal Properties of a High Rise Building Under Construction, *Proceedings of the 28th International Modal Analysis Conference*, February 1–4, 2010, Jacksonville, Florida, USA. Paper No. 242.

Park, H.S., H.M. Lee, H.M., Adeli, H., and Lee, I. (2007), A New Approach for Health Monitoring of Structures: Terrestrial Laser Scanning, *Computer-Aided Civil and Infrastructure Engineering*, 22:1, pp. 19-30.

SAP2000, 2006, *Linear and Nonlinear Static and Dynamic Analysis and Design of Three-Dimensional Structures.* Computers and Structures, Inc., California, USA, version 11.0.

Shahawy, M. A., and Arockiasamy, M. (1996), Field Instrumentation to Study the Time-Dependent Behavior in Sunshine Skyway Bridge. *Journal of Bridge Engineering, ASCE*, 1 (2), 76-86.

Soyoz, S. and Feng, M.Q. (2009), Long-Term Monitoring and Identification of Bridge Structural Parameters, *Computer-Aided Civil and Infrastructure Engineering*, 24:2, pp. 82-92.

Stivaros, P. C. and Halvorsen, G. T. (1990), Shoring/reshoring operations for multistory buildings, *ACI Structural Journal*, 87 (5), 589–96.

Umesha, P.K., Ravichandran, R., Sivasubramanian K. (2009), Crack detection and quantification in beams using wavelets, *Computer-Aided Civil and Infrastructure Engineering*, 24:8, pp. 593-607.

Fig. 1. Perspective view of Guangzhou New TV Tower in July 2009
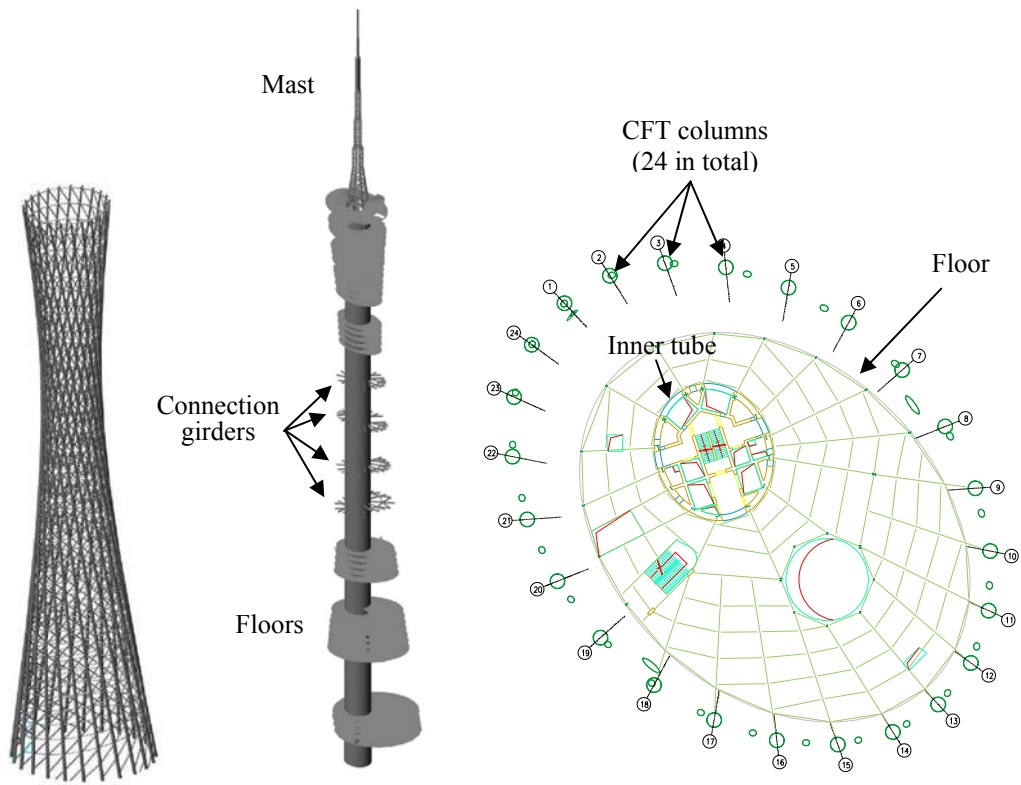
Fig. 2. The outer tube (left), the inner tube (middle), and a typical floor plan (right) for the Guangzhou New TV Tower

INNER TUBE   OUTER TUBE

Vibrating Wire Strain Gauge (12)   loop45   Vibrating Wire Strain Gauge (24)
SUB-STATION (1)   433.2m   Temperature Sensor (8)

Vibrating Wire Strain Gauge (12)   loop40   Vibrating Wire Strain Gauge (24)
SUB-STATION (1)   376.0m   Temperature Sensor (8)
Vibrating Wire Strain Gauge (12)   loop38   Vibrating Wire Strain Gauge (24)
SUB-STATION (1)   355.2m   Temperature Sensor (8)
Vibrating Wire Strain Gauge (12)   loop35   Vibrating Wire Strain Gauge (24)
SUB-STATION (1)   334.4m   Temperature Sensor (8)
Vibrating Wire Strain Gauge (12)   loop32   Vibrating Wire Strain Gauge (24)
SUB-STATION (1)   303.2m   Temperature Sensor (8)
Vibrating Wire Strain Gauge (12)   loop28   Vibrating Wire Strain Gauge (24)
SUB-STATION (1)   272.0m   Temperature Sensor (8)

Vibrating Wire Strain Gauge (12)   loop24   Vibrating Wire Strain Gauge (24)
SUB-STATION (1)   230.4m   Temperature Sensor (8)
Vibrating Wire Strain Gauge (12)   loop21   Vibrating Wire Strain Gauge (20)
SUB-STATION (1)   204.4m   Temperature Sensor (8)
Vibrating Wire Strain Gauge (12)   loop17   Vibrating Wire Strain Gauge (20)
SUB-STATION (1)   173.2m   Temperature Sensor (8)

Vibrating Wire Strain Gauge (12)   loop11   Vibrating Wire Strain Gauge (20)
SUB-STATION (1)   121.2m   Temperature Sensor (8)
Vibrating Wire Strain Gauge (12)   loop9   Vibrating Wire Strain Gauge (20)
SUB-STATION (1)   100.4m   Temperature Sensor (8)

Vibrating Wire Strain Gauge (12)   loop3   Vibrating Wire Strain Gauge (20)
Weather Station (1)   Temperature Sensor (8)
SUB-STATION (1)   32.8m   GPS Reference Station (1)
    Digital Camera (3)
    SUB-STATION (1)

Fig. 3. Layout of the strain monitoring system
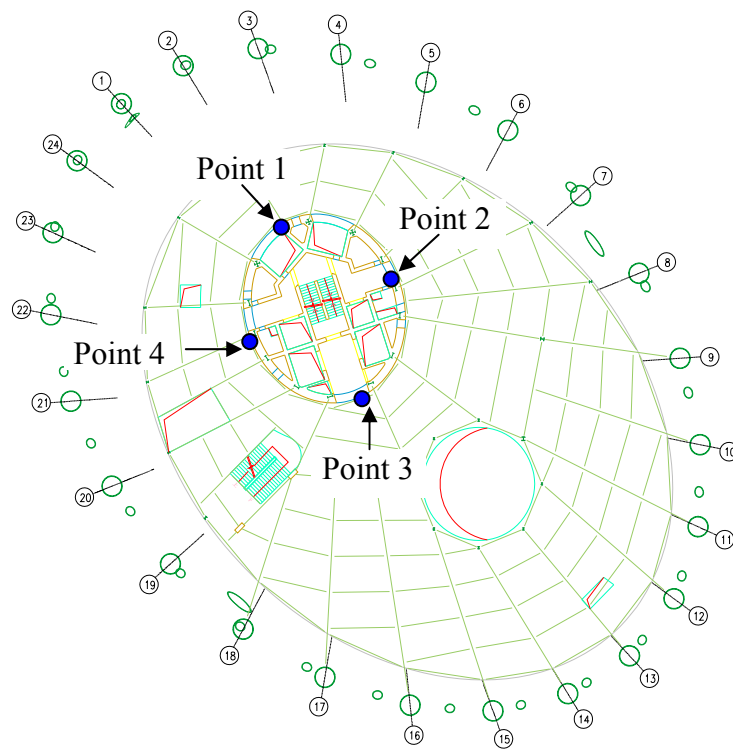
Fig. 4. Location of strain and temperature monitoring points in one critical section

(a) Original vibrating wire strain gauge

(b) Concrete coating
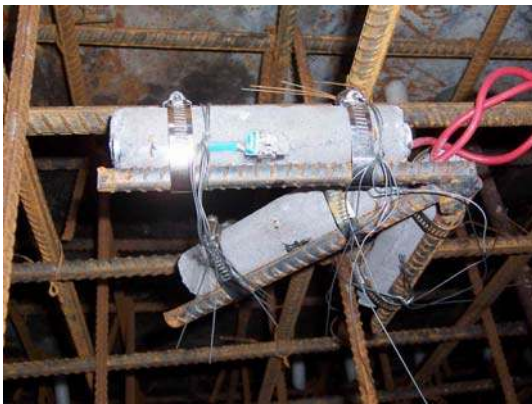
(c) A strain rosette in the inner tube

(d) Protection of cables

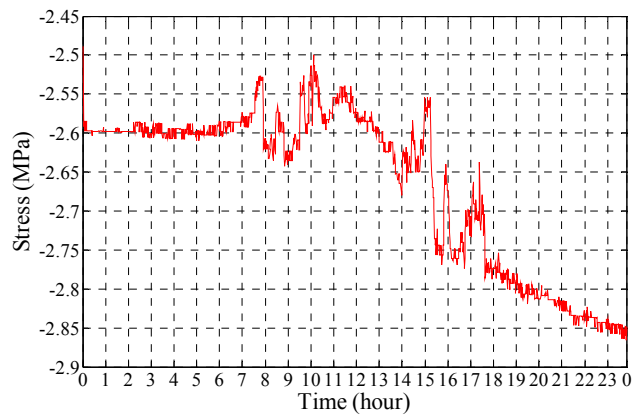Fig. 5. Installation of vibrating wires
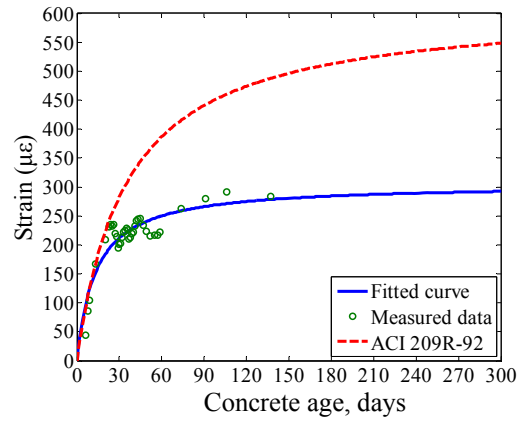
Fig. 6. Shrinkage of concrete
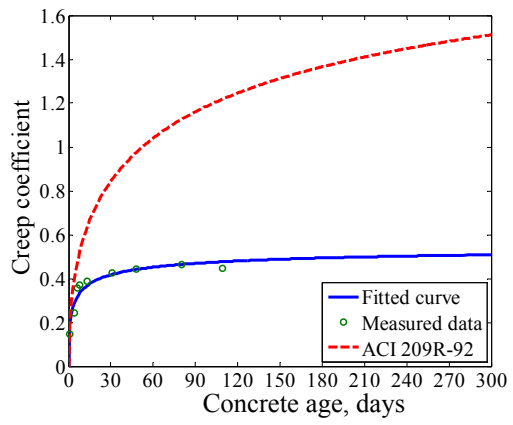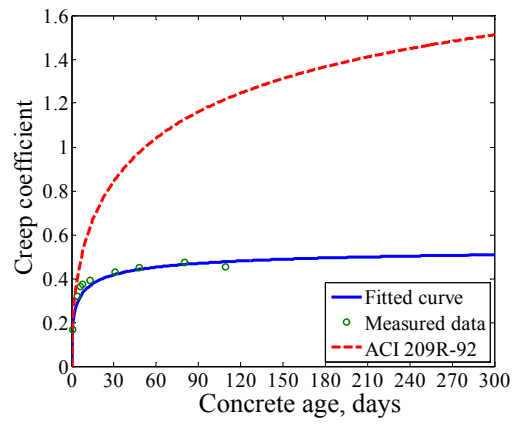
(a) Specimen 1   (b) Specimen 2

Fig. 7. Creep of concrete

Fig. 8a. One of the critical stages of construction

Fig. 8b. Principal stresses at the first connection level during the construction stage

(i) Principal stress at point 2 (204.4m)
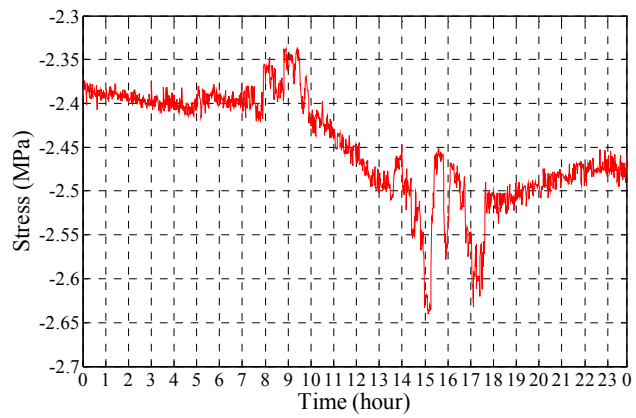
(ii) Principal stress at point 4 (204.4m)
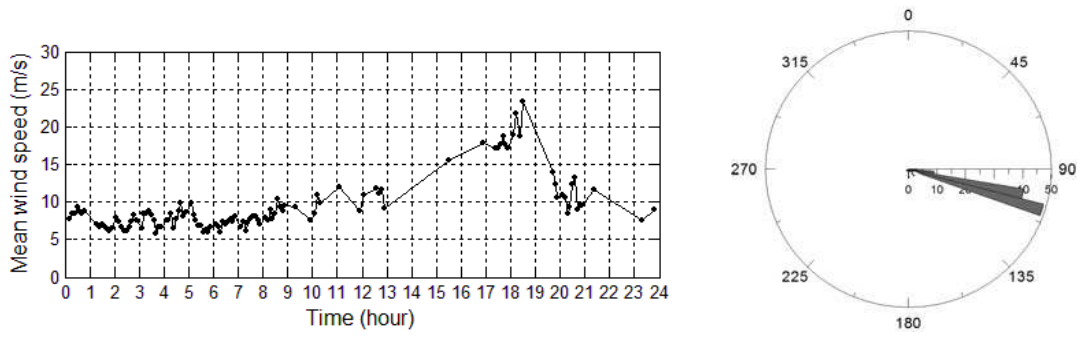
Fig. 9. Two-minute mean wind speed at the top of the tower (left) and wind rose

diagram (right) during Typhoon Neoguri on April 19, 2008
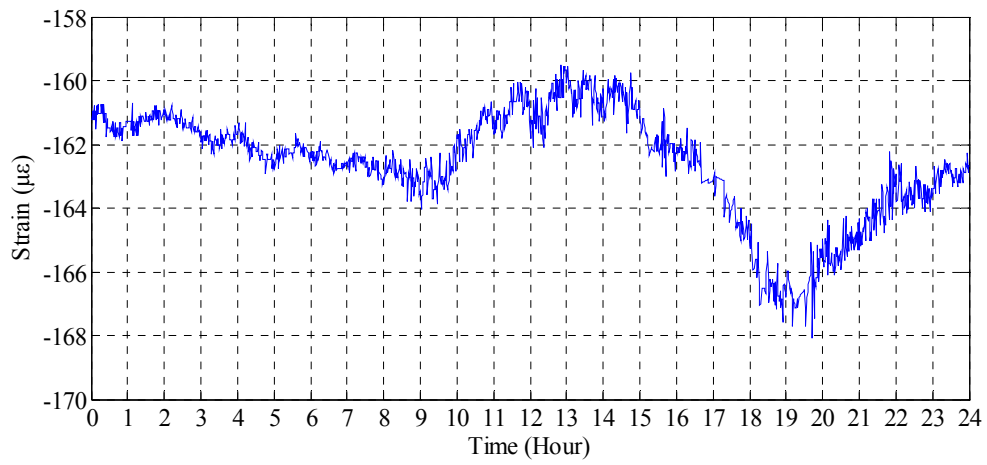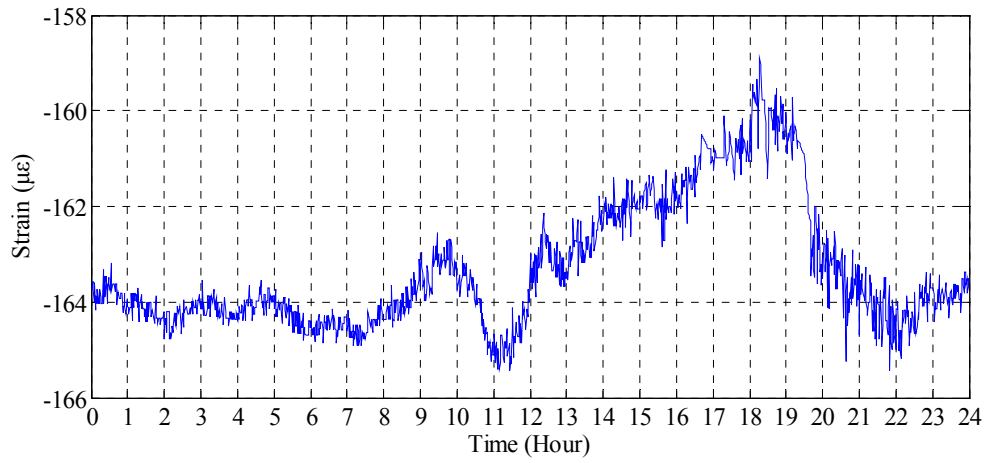
Fig. 10. Vertical strain responses at point 2 (upper) and point 4 (lower) at a height of

121.2 m during Typhoon Neoguri on April 19, 2008
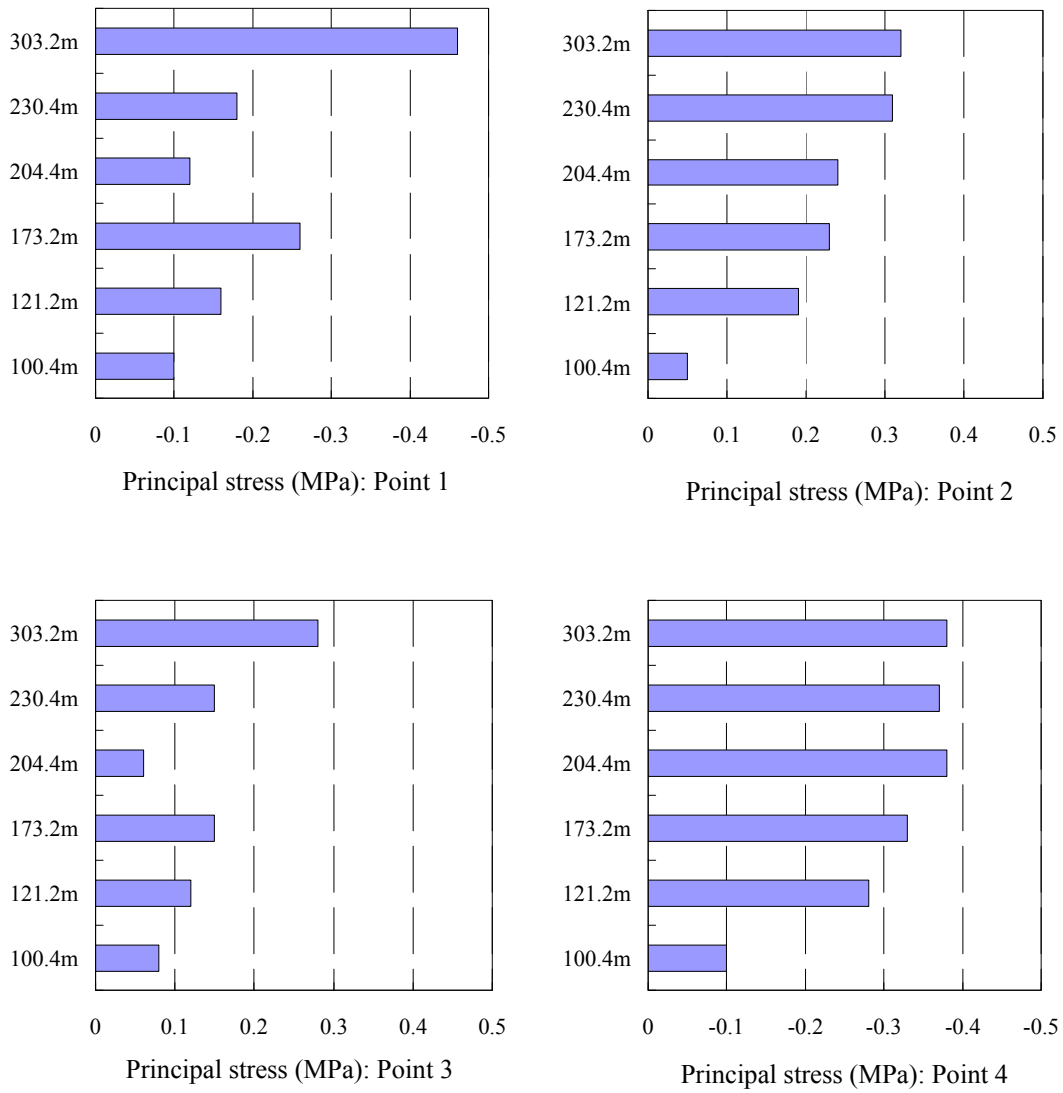
Fig. 11. Variation in principal stresses in different sections during Typhoon Neoguri on

April 19, 2008
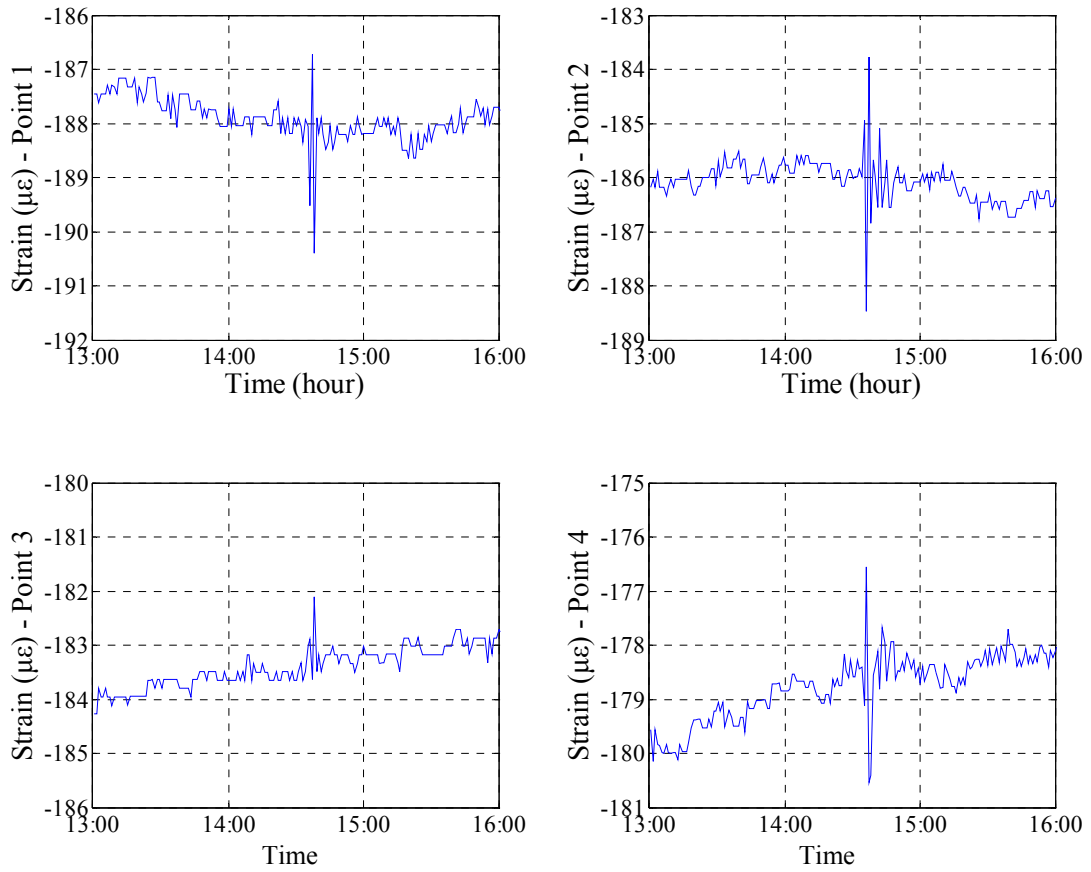
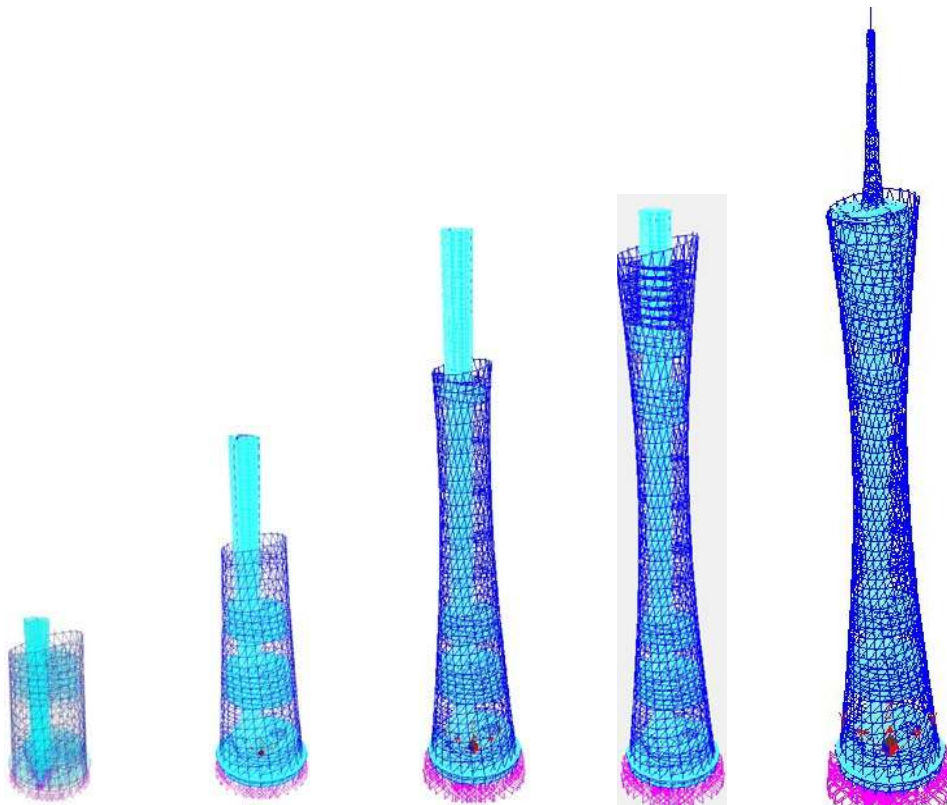Fig. 12. Vertical strain responses in the 121.2 m section during the Wenchuan
Earthquake on May 12, 2009
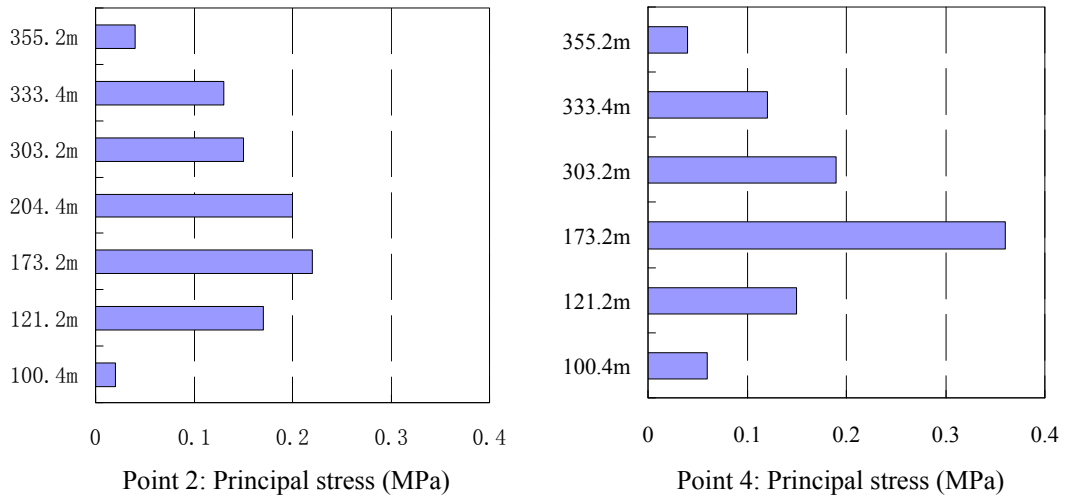
Fig. 13. Variation in the principal stresses in different sections during the Wenchuan

Earthquake on 12 May 2009

| 2007.07 | 2007.12 | 2008.06 | 2008.10 | 2009.07 |

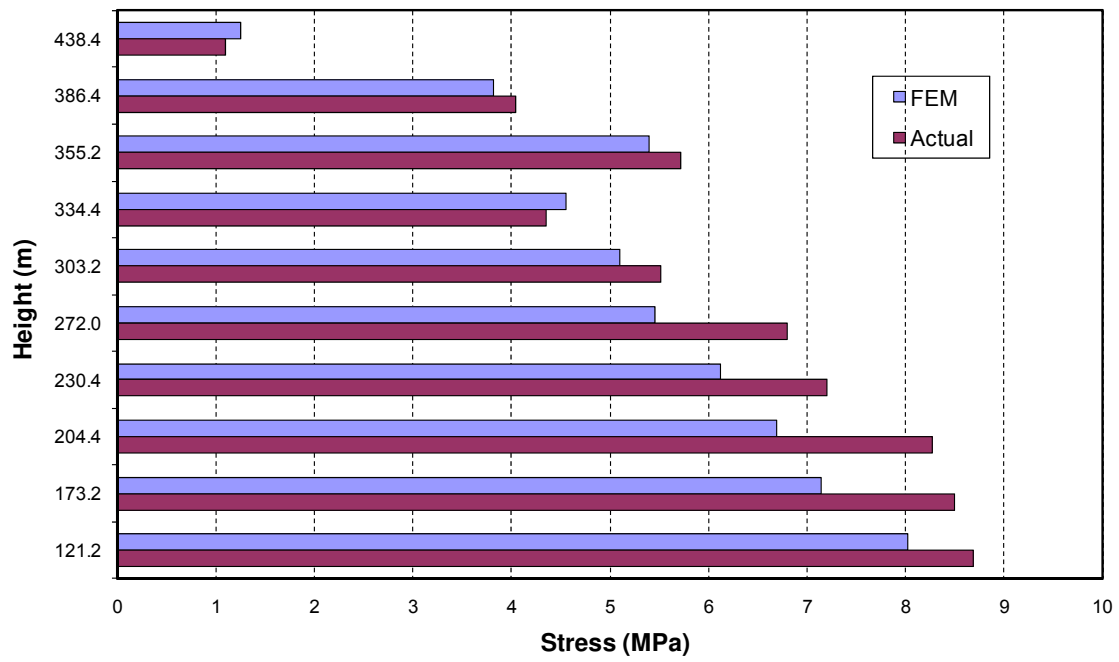Fig. 14. Photographs of the tower and the corresponding FE models at different stages

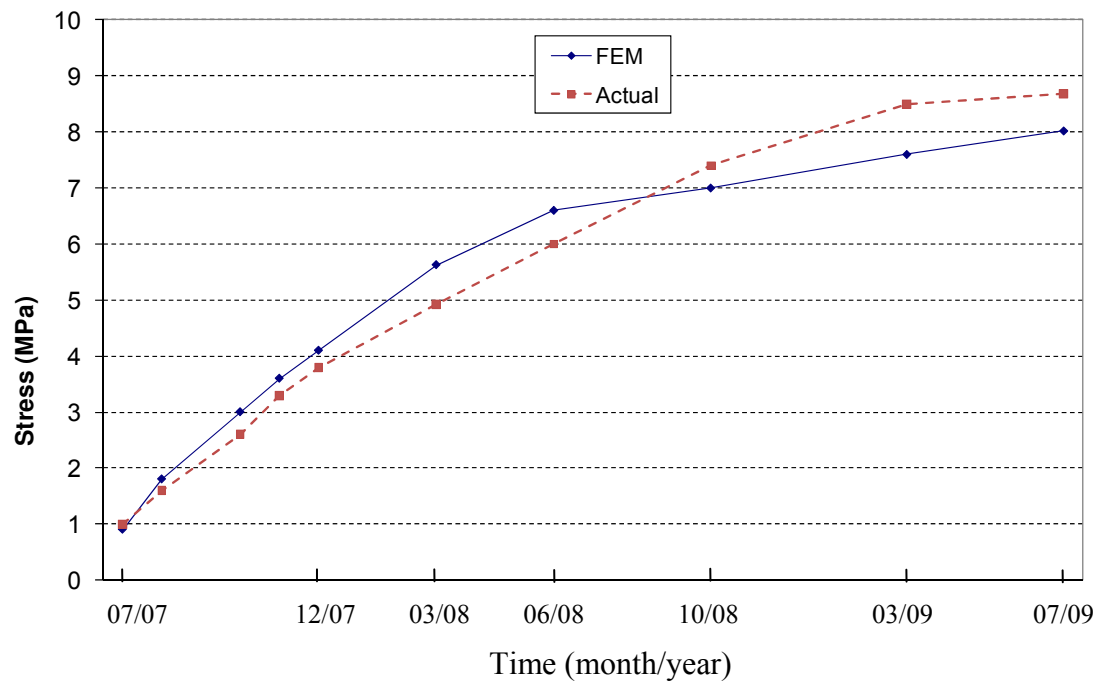Fig. 15. Stress distribution in different sections: point 2 in July 2009

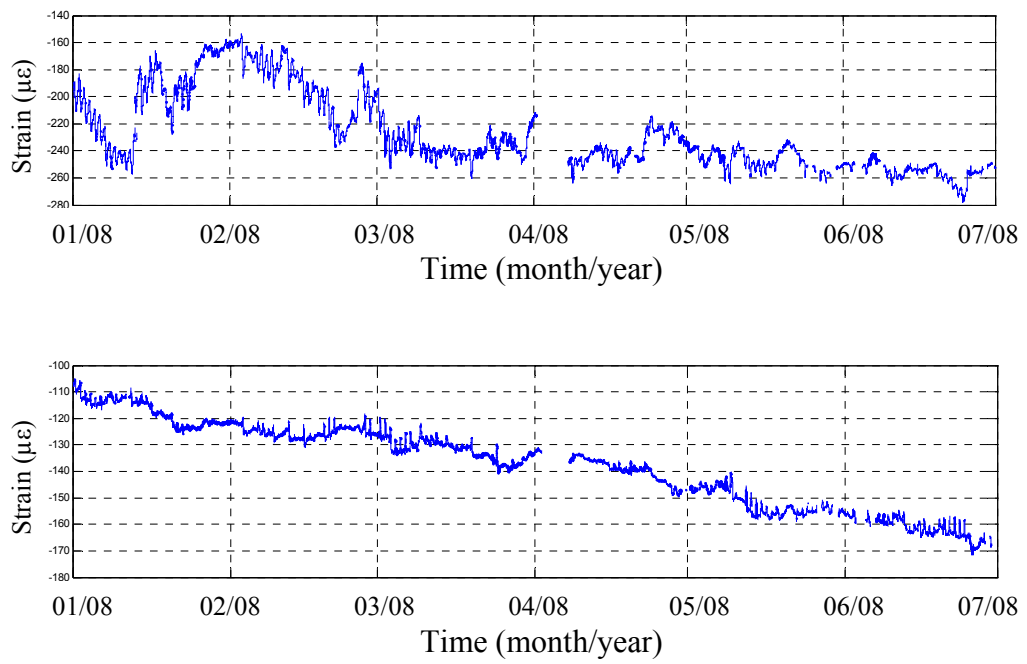Fig. 16. Stress evolution at different stages of construction: Point 2 at the 121.2 m level

Fig. 17. Vertical strains measured at point 2 at the 32.8 m level (upper) and at point 2 at

the 121.2 m level (lower)